Improved lumped models for transient combined convective and radiative cooling of multi-layer composite slabs

Chen An [a], Jian Su [b],*

[a] Ocean Engineering Program, COPPE, Universidade Federal do Rio de Janeiro, CP 68508, Rio de Janeiro, 21941-972, Brazil
[b] Nuclear Engineering Program, COPPE, Universidade Federal do Rio de Janeiro, CP 68509, Rio de Janeiro, 21941-972, Brazil

ABSTRACT

Improved lumped parameter models were developed for the transient heat conduction in multi-layer composite slabs subjected to combined convective and radiative cooling. The improved lumped models were obtained through two-point Hermite approximations for integrals. Transient combined convective and radiative cooling of three-layer composite slabs was analyzed to illustrate the applicability of the proposed lumped models, with respect to different values of the Biot numbers, the radiation-conduction parameter, the dimensionless thermal contact resistances, the dimensionless thickness, and the dimensionless thermal conductivity. It was shown by comparison with numerical solution of the original distributed parameter model that the higher order lumped model ($H_{1,1}/H_{0,0}$ approximation) yielded significant improvement of average temperature prediction over the classical lumped model. In addition, the higher order ($H_{1,1}/H_{0,0}$) model was applied to analyze the transient heat conduction problem of steel-concrete-steel sandwich plates.

© 2011 Elsevier Ltd. All rights reserved.

1. Introduction

Transient heat conduction problem in multi-layer composite slabs has been extensively studied due to its applications in various technological areas such as dynamical thermal behavior of walls, working regime of heat treatment furnace, thermally protected structures, transient aerodynamic heating of airborne vehicles, and heat transfer in insulation materials [1–8]. Many analytical and numerical approaches have been proposed to obtain the transient response of one-dimensional multi-layer composite conducting slabs with convective cooling boundary conditions. De Monte [9,10] reviewed a historical bibliography and presented a 'natural' analytic approach simplifying the eigenvalues solving process by placing the thermal diffusivity on the time-dependent function side in the form of separated variables. Blanc and Touratier [5] presented a constrained discrete layer model as an approximated solution, in which the interface conditions for heat flux are incorporated into the governing equation of each layer in order to reduce the number of unknowns. Chen and Wang [11,12] estimated the heat gain/loss through building multi-layer constructions using a frequency-domain regression method based on the theoretical frequency-response characteristics of the walls. Oturanç and Sahin [6] solved the transient heat conduction problem in two-layer

composite wall analytically using spectral analysis, where an asymptotic formula is derived for the eigenvalues of the spectral problem. Antonopoulos et al. [13] applied orthogonal expansion of functions over multi-layer walls to obtain an analytical solution for on-site estimation of the layer thermal properties of multi-layer walls, referred to as the inverse wall heat conduction problem. Based on finite difference method, Charette et al. [4] and Asan [1] analyzed the heat conduction problem in a composite medium with variable thermal properties and investigated the optimum insulation position from maximum time lag and minimum decrement factor point of view, respectively.

The analysis of transient conduction of multi-layer systems is more complicated when radiative cooling or heating at the boundaries is considered. Sundén [14] presented numerical solutions based on finite difference method of the thermal response of a composite slab subjected to a time-varying incident heat flux on one side and combined convective and radiative cooling on the other side. Miller and Weaver [15] developed an analytical model based on separation of variables technique to predict the temperature distribution through a multi-layer composite structure subjected to combined convection and linearized radiation boundary conditions. To predict the effective thermal conductivities for multi-layer thermal insulations for high temperature fuel cell applications, Spinnler et al. [7] performed experimental study using a new design of guarded hot plate apparatus and solved the combined conduction and radiation heat transfer problem theoretically based on the

Nomenclature

Bi_1	Biot number at the left-side boundary surface
Bi_2	Biot number at the right-side boundary surface
c_{pi}	specific heat for the i-th layer
h_1	convective heat transfer coefficient at the left-side boundary surface
h_2	convective heat transfer coefficient at the right-side boundary surface
k_i	thermal conductivity for the i-th layer
k_{ref}	reference thermal conductivity
L	total thickness of multi-layer composite slabs
M	number of layers
N_{rc}	radiation-conduction parameter
Rc_i	thermal contact resistances at the inner boundary surfaces
Rc_i^*	dimensionless thermal contact resistances at the inner boundary surfaces
t	time
T_0	uniform initial temperature of multi-layer composite slabs
T_a	adiabatic surface temperature
T_f	right-side environmental fluid temperature
T_i	temperature for the i-th layer
T_m	left-side environmental fluid temperature
T_s	radiation sink temperature
x	space coordinate
x_1	value of the space coordinate at the left-side boundary surface
x_i	values of the space coordinate at the inner boundary surfaces
x_{M+1}	value of the space coordinate at the right-side boundary surface

Greek Letters

α_i	thermal diffusivity for the i-th layer
α_{ref}	reference thermal diffusivity
δ_i	dimensionless thickness for the i-th layer
ϵ	surface emissivity
η	dimensionless space coordinate
η_1	value of the dimensionless space coordinate at the left-side boundary surface
η_i	values of the dimensionless space coordinate at the inner boundary surfaces
η_{M+1}	value of the dimensionless space coordinate at the right-side boundary surface
θ_a	dimensionless adiabatic surface temperature
θ_i	dimensionless temperature for the i-th layer
θ_m	dimensionless left-side environmental fluid temperature
κ_i	dimensionless thermal diffusivity for the i-th layer
λ_i	dimensionless thermal conductivity for the i-th layer
ρ_i	density for the i-th layer
σ	Stefan–Boltzmann constant
τ	dimensionless time

Subscripts

i	i-th layer defined in the domain
avi	average for the i-th layer

energy conservation equation approach together with a scaling model. Besides, Li and Cheng [8] applied energy balance equation to obtain a mathematical model for the combined radiation and conduction heat transfer in multi-layer perforated insulation material using in space, which was solved numerically by iterative method combining with the alternating directions implicit method.

The lumped parameter approach has been widely used to analyze the dynamical thermal behavior of structures [16–21]. A simplified formulation of the transient heat conduction extremely useful and sometimes even mandatory as in the analysis of other complex thermal systems. Due to the inherent limitation of the classical lumped parameter approach, improved lumped models have been developed by different approaches [22–27]. Cotta and Mikhailov [22] proposed a systematic formalism to provide improved lumped parameter formulation for steady and transient heat conduction problems based on Hermite approximation for integrals that define averaged temperatures and heat fluxes. This approach has been shown to be efficient in a great variety of practical applications [28–32]. In this work, we present improved lumped models for transient combined convective and radiative cooling of multi-layer composite slabs, extending previous works on the particular cases of a single slab subjected to convective cooling [23], radiative cooling [24], and combined convective-radiative cooling [32]. The proposed lumped models are obtained through two-point Hermite approximations for integrals [33,22]. By comparing with numerical solution of the original distributed parameter formulation, it is shown that the higher order improved lumped model ($H_{1,1}/H_{0,0}$ approximation) yields significant improvement of average temperature prediction over the classical lumped model. In addition, the higher order ($H_{1,1}/H_{0,0}$) model is applied to analyze the transient heat conduction problem of steel-concrete-steel sandwich plates.

2. The mathematical formulation

Consider one-dimensional transient heat conduction in multi-layer composite slabs consisting of M parallel layers in cartesian coordinates, subjected to convective heat transfer at the left side and combined convective and radiative heat transfer at the right side, as shown in Fig. 1. The layers are labeled as 1 to M from the left to right. Let x be the coordinate perpendicular to the layers, x_i, $i = 1, 2, ..., M$, represent its value at the left surface of each
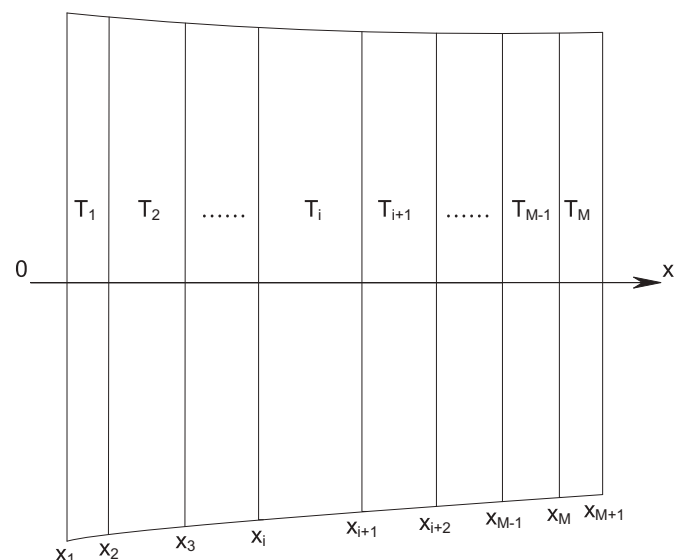

Fig. 1. Illustration of M-layer composite slabs.

layer, and x_{M+1} be the coordinate value at the right surface of M-th layer. It is assumed that the thermophysical properties of the layers are homogeneous, isotropic and independent of the temperature. There is no volumetric heat generation in the slabs. The thermal contact resistance between adjacent i-th and $(i+1)$-th layer at interface x_{i+1}, $i = 1, 2, ..., M-1$, is represented by Rc_i. Initially, all the layers are at a specified uniform temperature T_0. At $t = 0$, the composite is exposed to an environment of a constant fluid temperature T_m with a constant convective heat transfer coefficient h_1 at the left side, and an environment of a constant fluid temperature T_f with a constant heat transfer coefficient h_2 and a constant radiation sink temperature T_s at the right side.

The mathematical formulation of the one-dimensional transient heat conduction problem is given by

$$\frac{\partial T_i}{\partial t} = \alpha_i \frac{\partial^2 T_i}{\partial x^2}, \quad in \ \ x_i < x < x_{i+1}, \ \ i = 1, 2, ..., M, \ \ for \ \ t > 0, \quad (1)$$

with the following boundary and interface conditions

$$-k_1 \frac{\partial T_1}{\partial x} = h_1 (T_m - T_1), \quad at \ \ x = x_1, \ \ for \ \ t > 0, \quad (2)$$

$$-k_M \frac{\partial T_M}{\partial x} = h_2 \left(T_M - T_f \right) + \epsilon\sigma \left(T_M^4 - T_s^4 \right), at \ x = x_{M+1}, for \ t > 0, \quad (3)$$

$$-k_i \frac{\partial T_i}{\partial x} = \frac{T_i - T_{i+1}}{Rc_i}, \quad at \ \ x = x_{i+1}, \ \ i = 1, 2, ..., M-1, \ \ for \ \ t > 0, \quad (4)$$

$$k_i \frac{\partial T_i}{\partial x} = k_{i+1} \frac{\partial T_{i+1}}{\partial x}, \quad at \ \ x = x_{i+1}, \ \ i = 1, 2, ..., M-1, \ \ for \ \ t > 0, \quad (5)$$

and the initial conditions for each layer

$$T_i(x,0) = T_0, \quad in \ \ x_i < x < x_{i+1}, \ \ i = 1, 2, ..., M, \ \ at \ \ t = 0, \quad (6)$$

where $T_i(x,t)$ is the temperature in the i-th layer, t the time, $\alpha_i (= k_i / \rho_i c_{pi})$ the thermal diffusivity, k_i the thermal conductivity, ρ_i the density, c_{pi} the specific heat, ϵ the surface emissivity, and σ the Stefan–Boltzmann constant.

It should be noted that in general the environmental fluid temperature T_f differs from the radiation sink temperature T_s. It is convenient to introduce the adiabatic surface temperature T_a, defined by

$$h_2 \left(T_a - T_f \right) + \epsilon\sigma \left(T_a^4 - T_s^4 \right) = 0 \quad (7)$$

The boundary condition Eq. (3) can be rewritten with use of the adiabatic surface temperature

$$-k_M \frac{\partial T_M}{\partial x} = h_2 (T_M - T_a) + \epsilon\sigma \left(T_M^4 - T_a^4 \right), at \ x = x_{M+1}, for \ t > 0, \quad (8)$$

The mathematical formulation given by the system of Eqs. (1,2,4–6,8) can now be expressed in dimensionless form as follows:

$$\frac{\partial \theta_i}{\partial \tau} = \kappa_i \frac{\partial^2 \theta_i}{\partial \eta^2}, \quad in \ \ \eta_i < \eta < \eta_{i+1}, \ \ i = 1, 2, ..., M, \ \ for \ \ \tau > 0, \quad (9)$$

$$-\lambda_1 \frac{\partial \theta_1}{\partial \eta} = Bi_1 (\theta_m - \theta_1), \quad at \ \ \eta = \eta_1, \ \ for \ \ \tau > 0, \quad (10)$$

$$-\lambda_M \frac{\partial \theta_M}{\partial \eta} = Bi_2 (\theta_M - \theta_a) + Nrc \left(\theta_M^4 - \theta_a^4 \right), at \ \ \eta = \eta_{M+1}, for \ \tau > 0, \quad (11)$$

$$-\lambda_i \frac{\partial \theta_i}{\partial \eta} = \frac{\theta_i - \theta_{i+1}}{Rc_i^*}, \quad at \ \ \eta = \eta_{i+1}, \ \ i = 1, 2, ..., M-1, \ \ for \ \tau > 0, \quad (12)$$

$$\lambda_i \frac{\partial \theta_i}{\partial \eta} = \lambda_{i+1} \frac{\partial \theta_{i+1}}{\partial \eta}, \quad at \ \ \eta = \eta_{i+1}, \ \ i = 1, 2, ..., M-1, \ \ for \ \tau > 0, \quad (13)$$

$$\theta_i(\eta, 0) = 1, \quad in \ \ \eta_i < \eta < \eta_{i+1}, \ \ i = 1, 2, ..., M, \ \ at \ \ \tau = 0, \quad (14)$$

where the dimensionless parameters are defined by

$$\theta_i = \frac{T_i}{T_0}, \quad \eta = \frac{x}{L}, \quad \eta_i = \frac{x_i}{L}, \quad \tau = \frac{\alpha_{ref} t}{L^2}, \quad (15a-d)$$

$$\kappa_i = \frac{\alpha_i}{\alpha_{ref}}, \quad \lambda_i = \frac{k_i}{k_{ref}}, \quad Rc_i^* = \frac{Rc_i k_{ref}}{L}, \quad (15e-g)$$

$$Bi_1 = \frac{h_1 L}{k_{ref}}, \quad Bi_2 = \frac{h_2 L}{k_{ref}}, \quad Nrc = \frac{\epsilon\sigma L T_0^3}{k_{ref}}. \quad (15h-j)$$

Table 1
Comparison of lumped models against finite difference solution for dimensionless average temperatures $\theta_{av1}(\tau)$, $\theta_{av2}(\tau)$ and $\theta_{av3}(\tau)$ at the different dimensionless time for Case I-1 ($N_{rc} = 8$).

τ	FD solution	CLSA	$H_{0,0}/H_{0,0}$	$H_{1,1}/H_{0,0}$
$\theta_{av1}(\tau)$				
0.01	0.977077	0.977009	0.977835	0.977556
0.05	0.898266	0.893692	0.910351	0.903590
0.10	0.817321	0.798962	0.837296	0.824230
0.20	0.678372	0.632965	0.696711	0.682392
0.50	0.380030	0.313717	0.380668	0.379461
1.00	0.158777	0.118866	0.153442	0.157714
$\theta_{av2}(\tau)$				
0.01	0.996140	0.993741	0.996449	0.996593
0.05	0.937442	0.919931	0.929336	0.938978
0.10	0.843144	0.809985	0.824080	0.844829
0.20	0.675684	0.624875	0.647446	0.677444
0.50	0.365143	0.304330	0.340116	0.365632
1.00	0.153164	0.116282	0.140259	0.152645
$\theta_{av3}(\tau)$				
0.01	0.716278	0.681148	0.708231	0.716658
0.05	0.306139	0.287994	0.300078	0.302117
0.10	0.181484	0.184685	0.182581	0.179309
0.20	0.130650	0.139459	0.133520	0.131164
0.50	0.089373	0.089328	0.089214	0.089909
1.00	0.062863	0.060252	0.062170	0.062962

Table 2
Comparison of lumped models against finite difference solution for dimensionless average temperatures $\theta_{av1}(\tau)$, $\theta_{av2}(\tau)$ and $\theta_{av3}(\tau)$ at the different dimensionless time for Case I-2 ($N_{rc} = 32$).

| τ	FD Solution	CLSA	$H_{0,0}/H_{0,0}$	$H_{1,1}/H_{0,0}$
$\theta_{av1}(\tau)$				
0.01	0.977077	0.976943	0.978254	0.977785
0.05	0.898204	0.892134	0.911842	0.904224
0.10	0.816621	0.795372	0.837165	0.823686
0.20	0.676158	0.627851	0.694092	0.680044
0.50	0.377791	0.310529	0.378190	0.377199
1.00	0.157964	0.117991	0.152610	0.156905
$\theta_{av2}(\tau)$				
0.01	0.994634	0.990535	0.994885	0.995275
0.05	0.929677	0.908304	0.920166	0.931360
0.10	0.834630	0.798228	0.814498	0.836428
0.20	0.669535	0.616660	0.641059	0.671385
0.50	0.362661	0.301079	0.337694	0.363153
1.00	0.152380	0.115433	0.139523	0.151861
$\theta_{av3}(\tau)$				
0.01	0.629150	0.558417	0.614129	0.629616
0.05	0.266202	0.245696	0.260075	0.262252
0.10	0.170676	0.174214	0.172173	0.168900
0.20	0.128845	0.137187	0.131623	0.129458
0.50	0.088956	0.088711	0.088780	0.089489
1.00	0.062749	0.060108	0.062056	0.062847
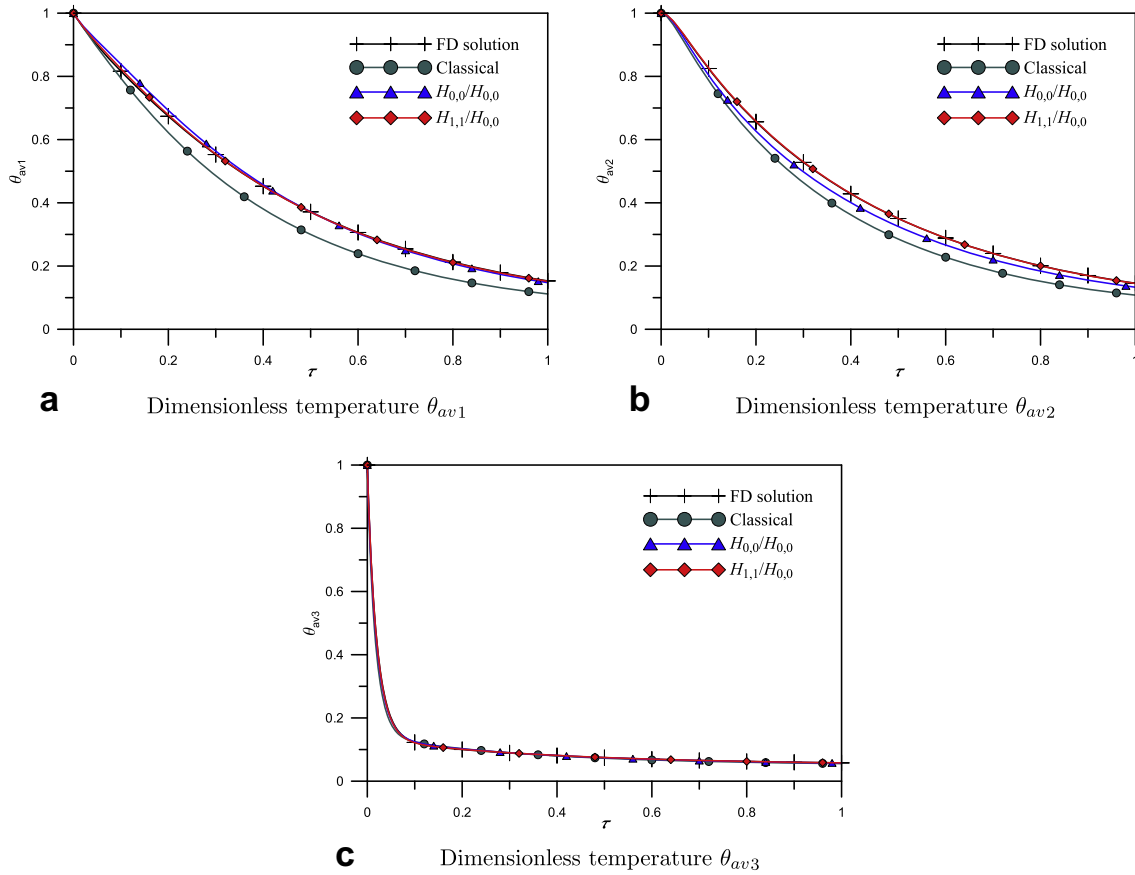
Fig. 2. Dimensionless temperature as a function of dimensionless time for each layer in Case II-3 ($Bi_2 = 20$).

Let δ_i represent the dimensionless thickness for each layer, $\delta_i = (x_{i+1} - x_i)/L$, $i = 1, 2, ..., M$, where the reference length L is chosen as the total thickness of composite slabs, $x_{m+1} - x_1$, hence we have

$$\sum_{i=1}^{M} \delta_i = 1. \tag{16}$$

The reference thermal conductivity and diffusivity can be taken as those of any layer, say, the second one, then $k_{ref} = k_2$ and $\alpha_{ref} = \alpha_2$. It can be seen that the problem is governed by the following dimensionless parameters, $Bi_1, Bi_2, N_{rc}, Rc_i^*, \lambda_i, \kappa_i, \delta_i, \theta_m$ and θ_a, $i = 1, 2, ..., M$. The radiation-conduction parameter, N_{rc} that governs the radiative cooling, is conceptually analog to the Biot numbers, Bi_1 and Bi_2, which are the governing parameters for an equivalent transient convective cooling.

3. Lumped models

Let us introduce the spatially averaged dimensionless temperature of the i-th layer as follows

$$\theta_{avi}(\tau) = \frac{1}{\eta_{i+1} - \eta_i} \int_{\eta_i}^{\eta_{i+1}} \theta_i(\eta, \tau) d\eta, \quad i = 1, 2, ..., M. \tag{17}$$

Operate Eqs. (9) by $\frac{1}{\eta_{i+1} - \eta_i} \int_{\eta_i}^{\eta_{i+1}} d\eta$ and using the definition of average temperatures, Eqs. (17), we have

$$\frac{d\theta_{avi}(\tau)}{d\tau} = \frac{\kappa_i}{\eta_{i+1} - \eta_i} \left(\left. \frac{\partial \theta_i}{\partial \eta} \right|_{\eta = \eta_{i+1}} - \left. \frac{\partial \theta_i}{\partial \eta} \right|_{\eta = \eta_i} \right), \quad i = 1, 2, ..., M. \tag{18}$$

Eqs. (18) are an equivalent integro-differential formulation of the original mathematical model, Eqs. (9), with no approximation involved.

Supposing that the temperature gradient is sufficiently smooth over each individual layer, the classical lumped system analysis (CLSA) is based on the assumption that the boundary temperatures can be reasonably well approximated by the average temperature, as

$$\theta_i(\eta, \tau)|_{\eta = \eta_i} \cong \theta_{avi}(\tau), \quad i = 1, 2, ..., M, \tag{19}$$

$$\theta_i(\eta, \tau)|_{\eta = \eta_{i+1}} \cong \theta_{avi}(\tau), \quad i = 1, 2, ..., M. \tag{20}$$

For each layer, there are two unknown boundary temperatures, $\theta_i|_{\eta=\eta_i}$ and $\theta_i|_{\eta=\eta_{i+1}}$, and two unknown heat fluxes, $\partial \theta_i/\partial \eta|_{\eta=\eta_i}$ and $\partial \theta_i/\partial \eta|_{\eta=\eta_{i+1}}$. Now, we have $2M$ equations provided by Eqs. (19, 20), $2(M-1)$ equations by Eqs. (12, 13) and two equations by Eqs. (10, 11), that are $4M$ equations for $4M$ unknowns which are solved to give the sought relations between the boundary temperatures and heat fluxes and the averaged temperatures in the multi-layer composite slabs. These relations are then used in the Eqs. (18) to yield the classical lumped model which is a closed-form expression with M ordinary differential equations for the averaged temperatures, to be solved with the initial conditions for the averaged temperatures

$$\theta_{avi}(0) = 1, \quad i = 1, 2, ..., M. \tag{21}$$

In an attempt to improve the approximation of the classical lumped model, we develop higher order lumped models by providing better relations between the boundary temperatures and the average temperatures, based on Hermite-type approximations
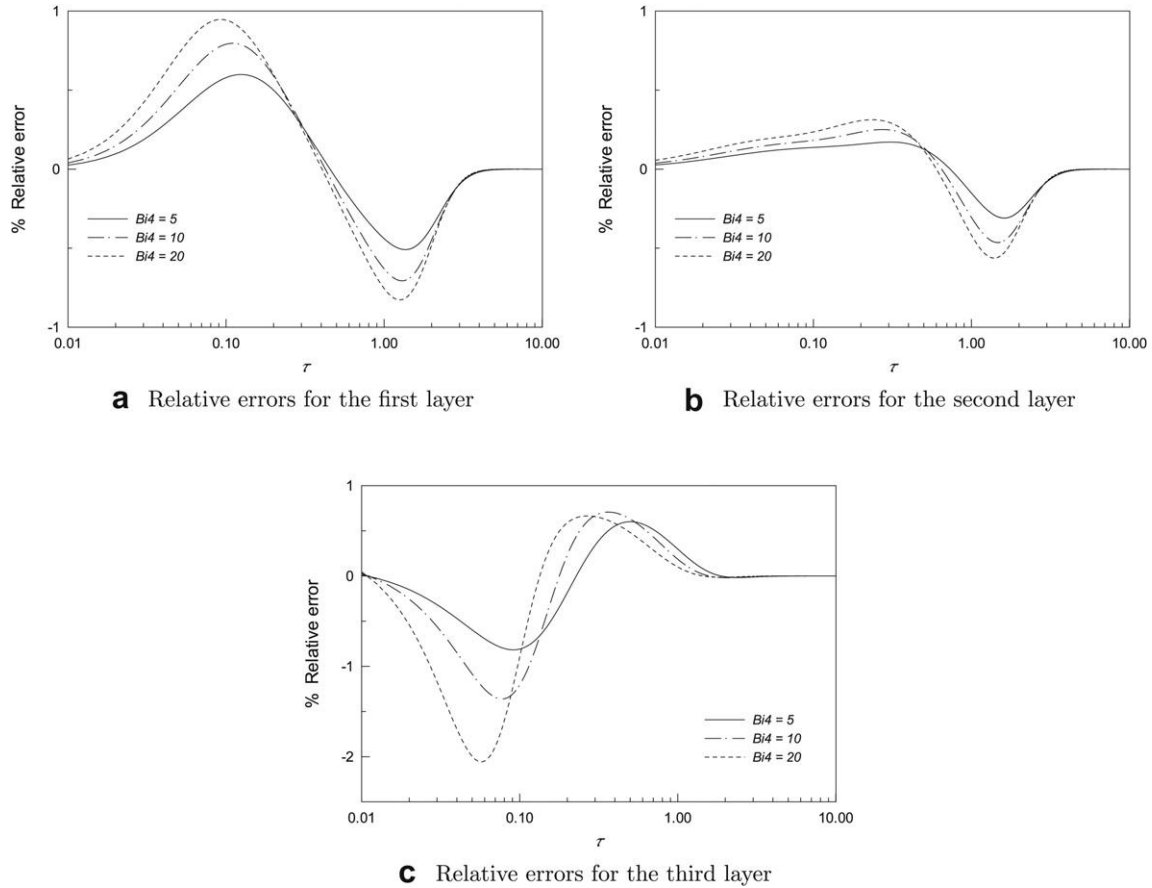
a Relative errors for the first layer

b Relative errors for the second layer

c Relative errors for the third layer

Fig. 3. Temporal variation of the relative errors for the average temperature predicted by the $H_{1,1}/H_{0,0}$ model, for various values of Bi_2.

for integrals that define the average temperatures and the heat fluxes. The general Hermite approximation for an integral, based on the values of the integrand and its derivatives at the integration limits, is written in the following form [33]:

$$\int_a^b y(x)\mathrm{d}x \cong \sum_{\nu=0}^{\alpha} C_\nu y^{(\nu)}(a) + \sum_{\nu=0}^{\beta} D_\nu y^{(\nu)}(b), \qquad (22)$$

where $y(x)$ and its derivatives $y^{(\nu)}(x)$ are defined for all $x \in (a, b)$. It is assumed that the numerical values of $y^{(\nu)}(a)$ for $\nu = 0, 1, ..., \alpha$, and $y^{(\nu)}(b)$ for $\nu = 0, 1, ..., \beta$ are available. The general expression for the $H_{\alpha,\beta}$ approximation is given by

$$\int_a^b y(x)\mathrm{d}x = \sum_{\nu=0}^{\alpha} C_\nu(\alpha, \beta) h^{\nu+1} y^{(\nu)}(a)$$
$$+ \sum_{\nu=0}^{\beta} C_\nu(\beta, \alpha)(-1)^\nu h^{\nu+1} y^{(\nu)}(b) + O\left(h^{\alpha+\beta+3}\right), \qquad (23)$$

where $h = b - a$, and

$$C_\nu(\alpha, \beta) = \frac{(\alpha+1)!(\alpha+\beta+1-\nu)!}{(\nu+1)!(\alpha-\nu)!(\alpha+\beta+2)!}. \qquad (24)$$

We first employ the plain trapezoidal rule in the integrals for both average temperatures and average heat fluxes ($H_{0,0}/H_{0,0}$ approximation), in the form

$$\theta_{avi}(\tau) \cong \frac{1}{2}\left[\theta_i(\eta, \tau)|_{\eta=\eta_i} + \theta_i(\eta, \tau)|_{\eta=\eta_{i+1}}\right], \quad i = 1, 2, ..., M, \qquad (25)$$

$$\int_{\eta_i}^{\eta_{i+1}} \frac{\partial\theta_i(\eta, \tau)}{\partial\eta}\mathrm{d}\eta = \theta_i(\eta, \tau)|_{\eta=\eta_{i+1}} - \theta_i(\eta, \tau)|_{\eta=\eta_i}$$
$$\cong \frac{\eta_{i+1} - \eta_i}{2}\left[\frac{\partial\theta_i}{\partial\eta}\bigg|_{\eta=\eta_i} + \frac{\partial\theta_i}{\partial\eta}\bigg|_{\eta=\eta_{i+1}}\right], \quad i = 1, 2, ..., M. \qquad (26)$$

Analytical solution of the $4M$ unknowns $\theta_i|_{\eta=\eta_i}$, $\theta_i|_{\eta=\eta_{i+1}}$, $\partial\theta_i/\partial\eta|_{\eta=\eta_i}$ and $\partial\theta_i/\partial\eta|_{\eta=\eta_{i+1}}$, $i = 1, 2, ..., M$, can be readily obtained from a closed system of Eqs. (10–13, 25, 26) by using a symbolic computation software such as *Mathematica*, and then used to close the ordinary differential equations Eqs. (18) for the average temperatures θ_{avi}, $i = 1, 2, ..., M$, to be solved with the initial condition Eqs. (21), providing the $H_{0,0}/H_{0,0}$ model.

Then we further improve the lumped model by employing two-side corrected trapezoidal rule in the integral for average temperatures, in the form

$$\theta_{avi}(\tau) \cong \frac{1}{2}\left[\theta_i(\eta, \tau)|_{\eta=\eta_i} + \theta_i(\eta, \tau)|_{\eta=\eta_{i+1}}\right]$$
$$+ \frac{\eta_{i+1} - \eta_i}{12}\left[\frac{\partial\theta_i}{\partial\eta}\bigg|_{\eta=\eta_i} - \frac{\partial\theta_i}{\partial\eta}\bigg|_{\eta=\eta_{i+1}}\right], \quad i = 1, 2, ..., M, \qquad (27)$$

while keeping the plain trapezoidal rule in the integral for heat fluxes ($H_{1,1}/H_{0,0}$ approximation).

Similarly, the boundary temperatures and heat fluxes can be obtained from Eqs. (10–13, 26, 27) and used to close the ordinary differential equations Eqs. (18) for the average temperatures, to be solved with the initial conditions Eqs. (21), providing the $H_{1,1}/H_{0,0}$ model.
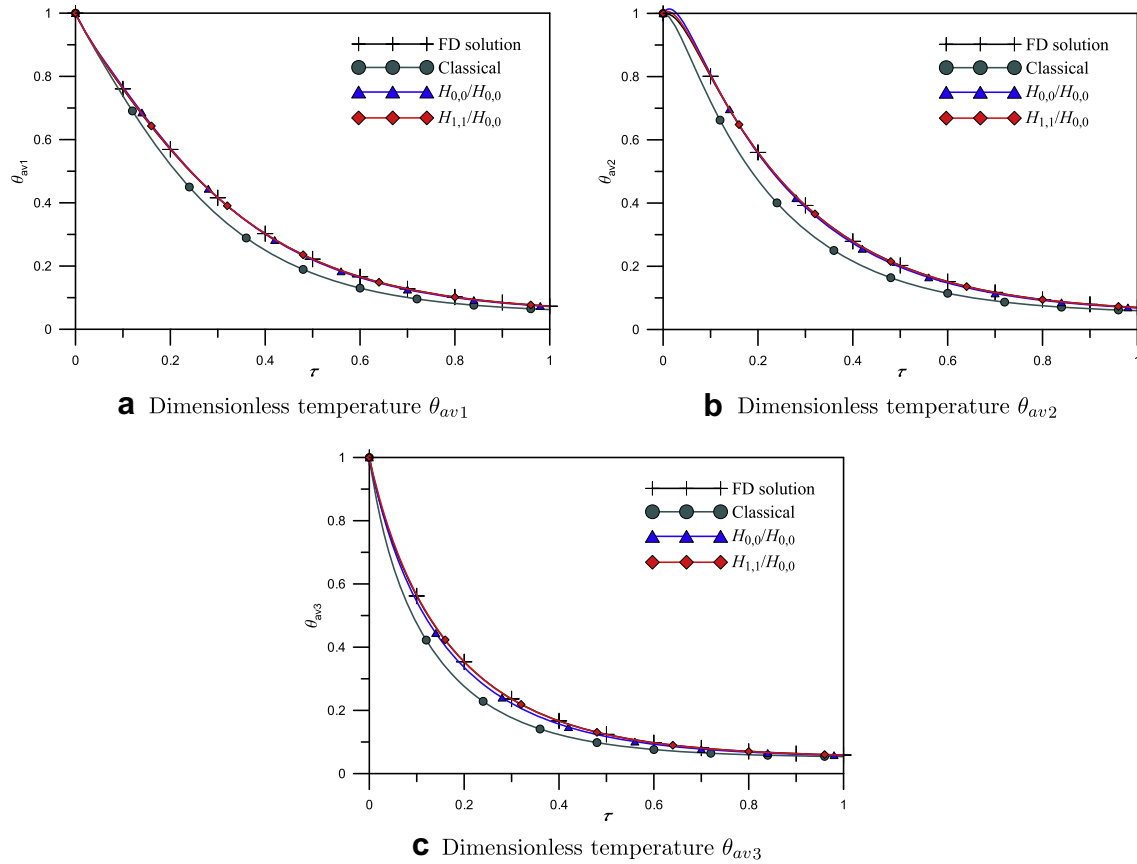
a Dimensionless temperature θ_{av1}

b Dimensionless temperature θ_{av2}

c Dimensionless temperature θ_{av3}

Fig. 4. Dimensionless temperature as a function of dimensionless time for each layer in Case III-1 ($\delta_3 = 0.7$).

4. Numerical results and discussions

Transient heat conduction in three-layer composite slabs with combined convective and radiative cooling is analyzed to illustrate the applicability of the proposed lumped models. The solutions of classical and improved lumped models are presented in tabular and graphical forms in comparison with a reference finite difference solution of the original distributed model, Eqs. (9–14). The initial boundary value problem defined by Eqs. (9–14) is solved by using an implicit finite difference method, with a 101 nodes mesh in spatial discretization for each layer and a dimensionless time step of 0.000001 for all cases. Different values of the Biot number Bi_2, the radiation-conduction parameter N_{rc}, dimensionless thermal contact resistances Rc_1^* and Rc_2^*, dimensionless thickness δ_3 and dimensionless thermal conductivity λ_3 are chosen so as to assess accuracy of the solutions obtained by the lumped models.

To make the expression concise, the examined problems with different cases are defined as follows:

Problem I. $Rc_1^* = 0.5$, $Rc_2^* = 0.5$, $Bi_2 = 12$, $\delta_1 = 0.2$, $\delta_2 = 0.6$, $\delta_3 = 0.2$, $\lambda_3 = 10$, $\kappa_3 = 5$. Case I-1: $N_{rc} = 8$; Case I-2: $N_{rc} = 32$.

Problem II. $Rc_1^* = 0.5$, $Rc_2^* = 0.5$, $N_{rc} = 5$, $\delta_1 = 0.2$, $\delta_2 = 0.6$, $\delta_3 = 0.2$, $\lambda_3 = 10$, $\kappa_3 = 5$. Case II-1: $Bi_2 = 5$; Case II-2: $Bi_2 = 10$; Case II-3: $Bi_2 = 20$.

Problem III. $Rc_1^* = 0.5$, $Rc_2^* = 0.5$, $Bi_2 = 10$, $N_{rc} = 5$, $\lambda_3 = 10$, $\kappa_3 = 5$. Case III-1: $\delta_1 = 0.15$, $\delta_2 = 0.15$, $\delta_3 = 0.7$; Case III-2: $\delta_1 = 0.05$, $\delta_2 = 0.05$, $\delta_3 = 0.9$.

Problem IV. $Rc_1^* = 0.5$, $Rc_2^* = 0.5$, $Bi_2 = 10$, $N_{rc} = 5$, $\delta_1 = 0.2$, $\delta_2 = 0.6$, $\delta_3 = 0.2$. Case IV-1: $\lambda_3 = 2$, $\kappa_3 = 1$; Case IV-2: $\lambda_3 = 1$, $\kappa_3 = 0.5$.

Problem V. $Bi_2 = 10$, $N_{rc} = 5$, $\delta_1 = 0.2$, $\delta_2 = 0.6$, $\delta_3 = 0.2$, $\lambda_3 = 10$, $\kappa_3 = 5$. Case V-1: $Rc_1^* = 0.1$, $Rc_2^* = 0.1$; Case V-2: $Rc_1^* = 10^{-7}$, $Rc_2^* = 10^{-7}$.

For all the problems tested, $Bi_1 = 1$, $\lambda_1 = 10$, $\lambda_2 = 1$, $\kappa_1 = 5$, $\kappa_2 = 1$, $\theta_m = 0.05$, $\theta_a = 0.05$, which are kept fixed in the following calculations.

Tables 1 and 2 present comparisons between the dimensionless average temperatures obtained by lumped models and the reference finite difference solution of the original distributed parameter model for each layer at the different dimensionless time, whose parameters are defined, respectively, by Case I-1 and Case I-2 in Problem I. As can be calculated at $\tau = 1.00$ in Case I-1, the classical lumped model gives errors of −25.137%, −24.080% and −4.153% for each layer, while the $H_{0,0}/H_{0,0}$ model gives errors of −3.360%, −8.426% and −1.102%, and the $H_{1,1}/H_{0,0}$ model yields −0.669%, −0.339% and 0.157%, respectively.

Fig. 2 presents the behaviors of the lumped models for Case II-3. It can be seen that the higher order lumped model ($H_{1,1}/H_{0,0}$ approximation) presents good agreement with the reference finite difference solution for values of Bi_2 as high as 20 and N_{rc} as high as 5. The overall error patterns for the proposed improved lumped model $H_{1,1}/H_{0,0}$ as a function of the logarithm of the dimensionless time are shown in Fig. 3. We can observe that for each case the error rises to maximum in early time, decays to zero in intermediate times, then reaches to the peak value in the opposite direction and finally diminishes to zero again in long times. The absolute values of the maximum relative errors for Case II-3 are around 0.95%, 0.55% and 2.05% respectively for each layer.

In Problem III, different values of the dimensionless thickness δ_3 are chosen in order to investigate the dimensionless temperature as a function of dimensionless time solved by the lumped models. In

a Dimensionless temperature θ_{av1}

b Dimensionless temperature θ_{av2}

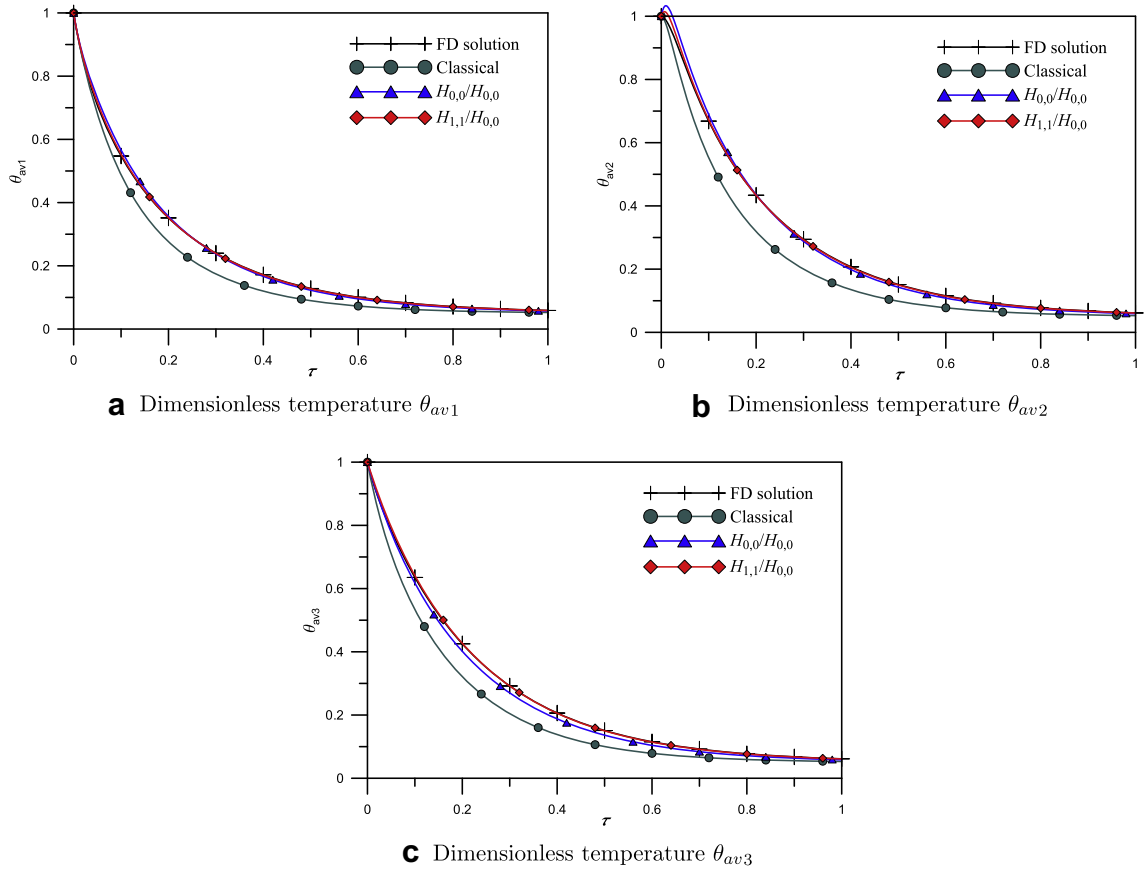**c** Dimensionless temperature θ_{av3}

Fig. 5. Dimensionless temperature as a function of dimensionless time for each layer in Case III-2 ($\delta_3 = 0.9$).

a Dimensionless temperature θ_{av1}
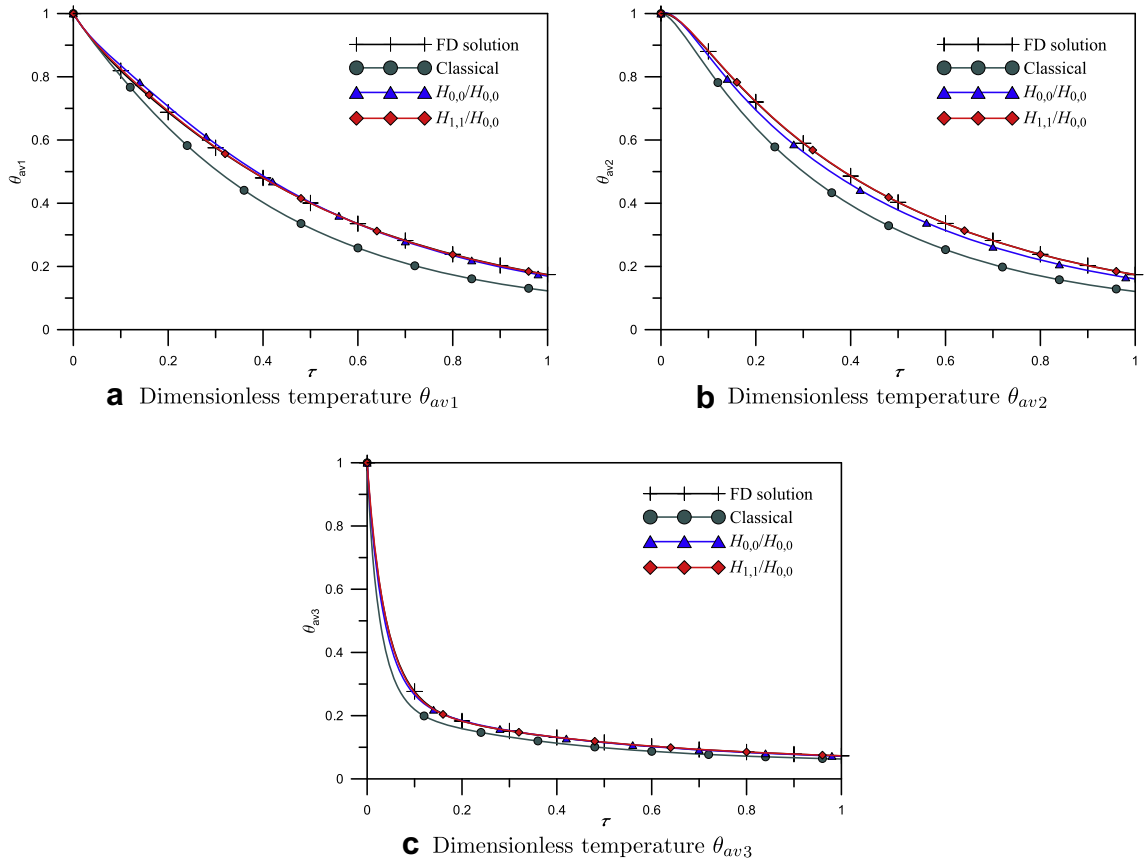

b Dimensionless temperature θ_{av2}

c Dimensionless temperature θ_{av3}

Fig. 6. Dimensionless temperature as a function of dimensionless time for each layer in Case IV-1 ($\lambda_3 = 2$, $\kappa_3 = 1$).
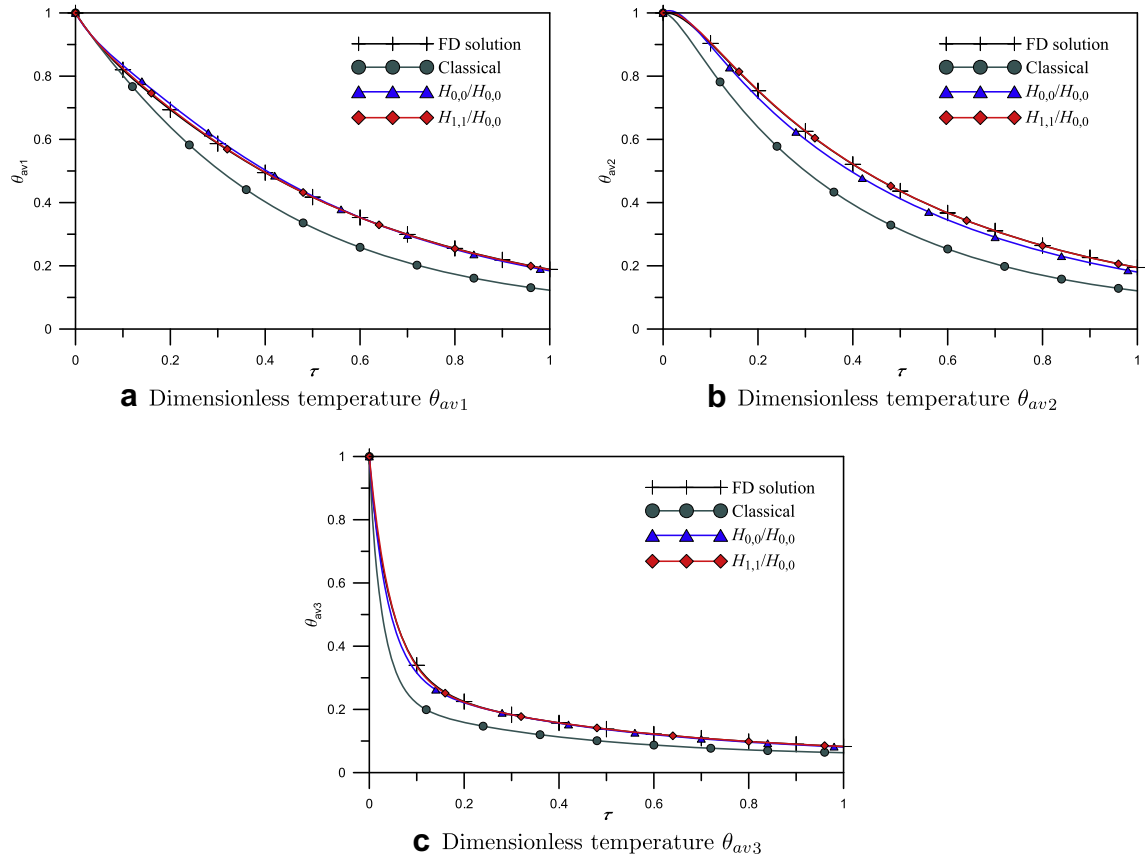
Fig. 7. Dimensionless temperature as a function of dimensionless time for each layer in Case IV-2 ($\lambda_3 = 1$, $\kappa_3 = 0.5$).
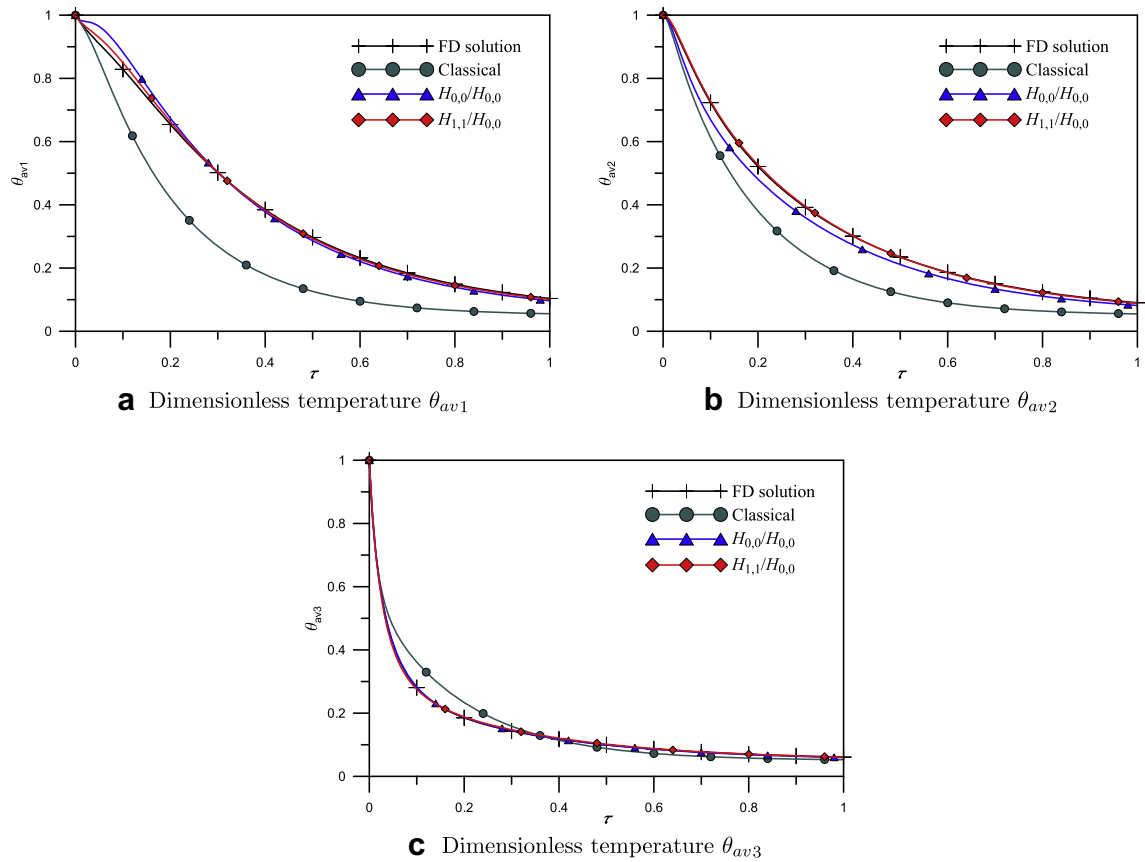

Fig. 8. Dimensionless temperature as a function of dimensionless time for each layer in Case V-1 ($Rc_1^* = 0.1$, $Rc_2^* = 0.1$).

a Dimensionless temperature θ_{av1}

b Dimensionless temperature θ_{av2}

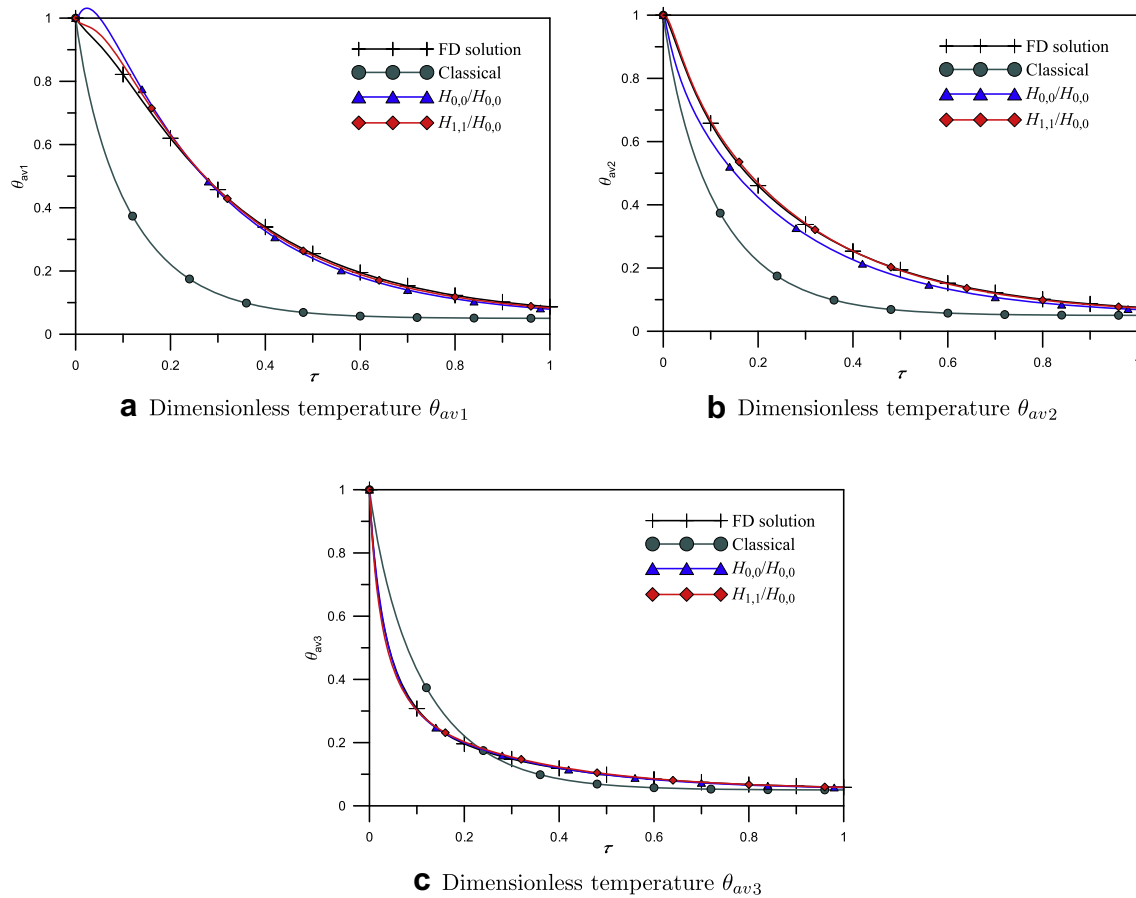**c** Dimensionless temperature θ_{av3}

Fig. 9. Dimensionless temperature as a function of dimensionless time for each layer in Case V-2 ($Rc_1^* = 10^{-7}$, $Rc_2^* = 10^{-7}$).

each case, the value of the dimensionless thickness δ_1 is assumed to be same as the value of δ_2. As shown in Figs. 4 and 5, although all the lumped models predict the correct value of the steady-state temperature for all the three layers, the classical lumped model gives larger relative errors for the whole time interval up to $\tau = 1$, while the improved lumped model $H_{0,0}/H_{0,0}$ presents smaller relative errors, and the $H_{1,1}/H_{0,0}$ model yields a good agreement with the finite difference solution. It is important to observe that as the value of the dimensionless thickness δ_3 increases, the improvement offered by the proposed models becomes more evident for the third layer compared with the above cases.

The numerical results of transient history for Case IV-1 and Case IV-2 are shown in Figs. 6 and 7. We can observe again that the averaged dimensionless temperature obtained by the improved lumped parameter formulation ($H_{1,1}/H_{0,0}$ approximation) is excellent agreement with the finite difference solution. It should be also noted that with the value of the dimensionless thermal conductivity λ_3 decreasing (the dimensionless thermal diffusivity κ_3 is directly proportional to λ_3), the improvement offered by the proposed models becomes more evident.

The next group of cases in Problem V are performed with the decreasing of the values of Rc_1^* and Rc_2^*, as shown in Figs. 8 and 9. Note that when the values of Rc_1^* and Rc_2^* reach to infinitesimal, imperfect contact interface boundary condition will convert to its special case that is perfect thermal contact condition at the interfaces. In Case V-2, $Rc_1^* = 10^{-7}$ and $Rc_2^* = 10^{-7}$ are utilized to simulate approximately the behaviors of the lumped models with perfect thermal contact conditions. Again, we can see that the prediction from the $H_{1,1}/H_{0,0}$ model appears clearly closer to the FD

solution than the results from the $H_{0,0}/H_{0,0}$ one, while the classical lumped model fails to give accurate results.

Finally, the higher order ($H_{1,1}/H_{0,0}$) model is employed to analyze the transient combined convective and radiative cooling of steel-concrete-steel sandwich plates, which present a common structure in engineering applications such as advanced nuclear reactors. The parameters used in this practical case are given in Table 3. The first and third layers are made of chrome steel (5% Cr), while the interlayer material is dry concrete. The corresponding Biot numbers and radiation-conduction parameter can be calculated from Eqs. (15) that $Bi_1 = 8$, $Bi_2 = 50$ and $N_{rc} \approx 3$. Fig. 10 shows the average temperature as a function of time for each layer of the sandwich plates. It can be clearly observed that before $t = 50$ s, the temperature of the third layer reduces to 400 K, while the first layer needs more than 600 s to reach the same temperature. The cooling of the concrete interlayer is slowest due to its higher thermal capacity and lower thermal conductivity.

Table 3
Parameters of steel-concrete-steel sandwich plates.

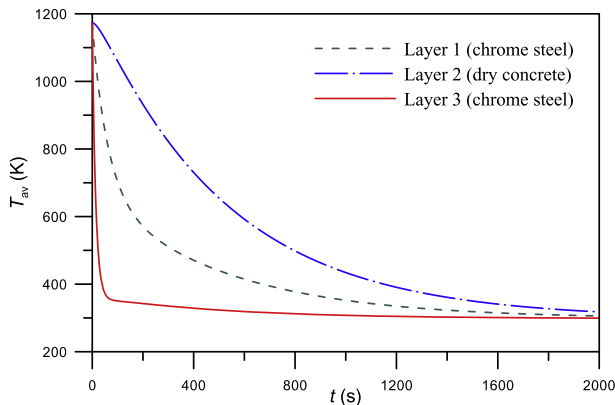| k_1	(W/m K)	40	ϵ		0.85
ρ_1	(kg/m³)	7833	Rc_1	(m²K/W)	0.005
c_{p1}	(J/kg K)	0.46	Rc_2	(m²K/W)	0.005
k_2	(W/m K)	1.28	h_1	(W/m²K)	204.8
ρ_2	(kg/m³)	2200	h_2	(W/m²K)	1280
c_{p2}	(J/kg K)	0.88	T_m	(K)	298
k_3	(W/m K)	40	T_f	(K)	298
ρ_3	(kg/m³)	7833	T_s	(K)	298
c_{p3}	(J/kg K)	0.46	T_0	(K)	1173

Fig. 10. Average temperature as a function of time for each layer of steel-concrete-steel sandwich plates.

5. Conclusions

Obtained through two-point Hermite approximations for integrals, improved lumped parameter models were developed for the transient heat conduction in multi-layer composite slabs subjected to combined convective and radiative cooling. Three-layer composite slabs were analyzed to illustrate the applicability of the proposed lumped models, with respect to different values of the Biot numbers, the radiation-conduction parameter, the dimensionless thickness, and the dimensionless thermal conductivity. It was shown by comparison with numerical solution of the original distributed parameter model that the higher order lumped model ($H_{1,1}/H_{0,0}$ approximation) yielded significant improvement of average temperature prediction over the classical lumped model, for radiation-conduction parameter as high as 32, and Biot number as high as 20. It was observed that the error rises to maximum in early time, decays to zero in intermediate times, then reaches to the peak value in the opposite direction and finally diminishes to zero again in long times. It was found that as value of the dimensionless thickness δ_3 increases or value of the dimensionless thermal conductivity λ_3 decreases, the improvement offered by the proposed models becomes more evident. For perfect thermal contact condition at the interfaces, it was found that the prediction from the $H_{1,1}/H_{0,0}$ model has a better agreement with the FD solution than the results from the $H_{0,0}/H_{0,0}$ one, while the classical lumped model fails to give accurate results. The analysis of transient combined convective and radiative cooling of steel-concrete-steel sandwich plates illustrates the potential applications of the proposed improved lumped model in practical engineering problems.

Acknowledgements

References

[1] H. Asan, Investigation of wall's optimum insulation position from maximum time lag and minimum decrement factor point of view, Energ. Buildings 32 (2) (2000) 197–203.
[2] H.T. Ozkahraman, A. Bolatturk, The use of tuff stone cladding in buildings for energy conservation, Constr. Build. Mater 20 (7) (2006) 435–440.
[3] M. Bouzidi, P. Duhamel, Non-stationary heat conduction in composite slabs with coupling. Application to enclosures: numerical computation of the analytical solution, Comput. Math. Appl. 11 (10) (1985) 1043–1055.
[4] A. Charette, R.T. Bui, G. Simard, The effect of stringent boundary-conditions on the solution of a transient heat-conduction problem, Math. Comput. Simulat 27 (1) (1985) 47–60.
[5] M. Blanc, M. Touratier, A constrained discrete layer model for heat conduction in laminated composites, Comput. Struct. 83 (2005) 1705–1718.
[6] G. Oturanç, A.Z. Sahin, Eigenvalue analysis of temperature distribution in composite walls, Int. J. Energ. Res. 25 (13) (2001) 1189–1196.
[7] M. Spinnler, E.R.F. Winter, R. Viskanta, Studies on high-temperature multilayer thermal insulations, Int. J. Heat Mass Tran 47 (6–7) (2004) 1305–1312.
[8] P. Li, H. Cheng, Thermal analysis and performance study for multilayer perforated insulation material used in space, Appl. Therm. Eng. 26 (16) (2006) 2020–2026.
[9] F. de Monte, Transient heat conduction in one-dimensional composite slab. a 'natural' analytic approach, Int. J. Heat Mass Tran 43 (19) (2000) 3607–3619.
[10] F. de Monte, An analytic approach to the unsteady heat conduction processes in one-dimensional composite media, Int. J. Heat Mass Tran 45 (6) (2002) 1333–1343.
[11] Y.M. Chen, S.W. Wang, Frequency-domain regression method for estimating ctf models of building multilayer constructions, Appl. Math. Model. 25 (7) (2001) 579–592.
[12] S.W. Wang, Y.M. Chen, A simple procedure for calculating thermal response factors and conduction transfer functions for multilayer walls, Appl. Therm. Eng. 22 (2002) 333–338.
[13] K.A. Antonopoulos, C. Tzivanidis, M. Vrachopoulos, Using orthogonal expansion of functions over multilayer walls for calculating the layer thermal properties, Appl. Therm. Eng. 17 (2) (1997) 193–201.
[14] B. Sundén, Transient heat-conduction in a composite slab by a time-varying incident heat-flux combined with convective and radiative cooling, Int. Commun. Heat Mass 13 (1986) 515–522.
[15] J.R. Miller, P.M. Weaver, Temperature profiles in composite plates subject to time-dependent complex boundary conditions, Compos. Struct. 59 (2) (2003) 267–278.
[16] K.A. Antonopoulos, E.P. Koronaki, Envelope and indoor thermal capacitance of buildings, Appl. Therm. Eng. 19 (1999) 743–756.
[17] K.A. Antonopoulos, E.P. Koronaki, Thermal parameter components of building envelope, Appl. Therm. Eng. 20 (2000) 1193–1211.
[18] P.E. Ergatis, P.G. Massouros, G.C. Athanasouli, G.P. Massouros, Time-dependent heat transfer coefficient of a wall, Int. J. Energ. Res. 27 (2003) 795–811.
[19] A.C.S. Estrada-Flores, D. Cleland, Prediction of the dynamic thermal behaviour of walls for refrigerated rooms using lumped and distributed parameter models, Int. J. Refrig 24 (2001) 272–284.
[20] P.T. Tsilingiris, On the thermal time constant of structural walls, Appl. Therm. Eng. 24 (5–6) (2004) 743–757.
[21] F. Alhama, J. Zueco, Application of a lumped model to solids with linearly temperature-dependent thermal conductivity, Appl. Math. Model. 31 (2) (2007) 302–310.
[22] R.M. Cotta, M.D. Mikhailov (Eds.), Heat Conduction - Lumped Analysis, Integral Transforms, Symbolic Computation, John Wiley & Sons, Chichester, England, 1997.
[23] J. Su, Improved lumped models for asymmetric cooling of a long slab by heat convection, Int. Commun. Heat Mass 28 (2001) 973–983.
[24] J. Su, Improved lumped models for transient radioactive cooling of a spherical body, Int. Commun. Heat Mass 31 (2004) 85–94.
[25] O. Bautista, F. Mendez, I. Campos, Transient heat conduction in a solid slab using multiple-scale analysis, Heat Mass Transf 42 (2005) 150–157.
[26] H. Sadat, A general lumped model for transient heat conduction in one-dimensional geometries, Appl. Therm. Eng. 25 (2005) 567–576.
[27] H. Sadat, A second order model for transient heat conduction in a slab with convective boundary conditions, Appl. Therm. Eng. 26 (2006) 962–965.
[28] C.R. Regis, R.M. Cotta, J. Su, Improved lumped analysis of transient heat conduction in a nuclear fuel rod, Int. Commun. Heat Mass 27 (2000) 357–366.
[29] J. Su, R.M. Cotta, Improved lumped parameter formulation for simplified lwr thermohydraulic analysis, Ann. Nucl. Energy 28 (2001) 1019–1031.
[30] N.J. Ruperti Jr., C.V. Falkenberg, R.M. Cotta, J. Su, Engineering analysis of ablative thermal protection for atmospheric reentry: improved lumped formulations and symbolic-numerical computation, Heat Transfer Eng. 25 (2004) 101–111.
[31] G. Su, Z. Tan, J. Su, Improved lumped models for transient heat conduction in a slab with temperature-dependent thermal conductivity, Appl. Math. Model. 33 (1) (2009) 274–283.
[32] Z. Tan, G. Su, J. Su, Improved lumped models for combined convective and radiative cooling of a wall, Appl. Therm. Eng. 29 (11–12) (2009) 2439–2443.
[33] J. Mennig, T. Auerbach, W. Hälg, Two point hermite approximation for the solution of linear initial value and boundary value problems, Comput. Method Appl. M. 39 (1983) 199–224.